NANO LETTERS

pubs.acs.org/NanoLett

Letter

Oriented Assembly of Lead Halide Perovskite Nanocrystals

Lili Liu,* Kyle Kluherz, Biao Jin, Daniel R. Gamelin, James J. De Yoreo, and Maria L. Sushko*

Cite This: *Nano Lett.* 2024, 24, 3299−3306

Read Online

ACCESS | Metrics & More | Article Recommendations | Supporting Information

ABSTRACT: Cesium lead halide nanostructures have highly tunable optical and optoelectronic properties. Establishing precise control in forming perovskite single-crystal nanostructures is key to unlocking the full potential of these materials. However, studying the growth kinetics of colloidal cesium lead halides is challenging due to their sensitivity to light, electron beam, and environmental factors like humidity. In this study, in situ observations of $CsPbBr_3$−particle dynamics were made possible through extremely low dose liquid cell transmission electron microscopy, showing that oriented attachment is the dominant pathway for the growth of single-crystal $CsPbBr_3$ architectures from primary nanocubes. In addition, oriented assembly and fusion of ligand-stabilized cubic $CsPbBr_3$ nanocrystals are promoted by electron beam irradiation or introduction of polar additives that both induce partial desorption of the original ligands and polarize the nanocube surfaces. These findings advance our understanding of cesium lead halide growth mechanisms, aiding the controlled synthesis of other perovskite nanostructures.

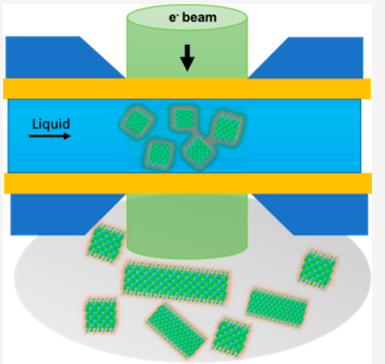

KEYWORDS: *cesium lead halide, oriented attachment, liquid phase TEM, ligand desorption, surface polarization*

Metal halide perovskites are promising materials for solar energy conversion because of their excellent optical and optoelectronic properties. Specifically, colloidal cesium lead halides ($CsPbX_3$, where X = Cl, Br, or I), which have relatively high thermal stability, show tunable broadband absorption, exhibit extremely high photoluminescence quantum yields, display relatively long optical and spin coherence, and are well-suited for integration into solar cells, light-emitting diodes, or other photonics architectures.[1−34] These unique properties have led to intense research in the fabrication of ordered $CsPbX_3$ nanoarchitectures with tunable properties that depend on the nanoscale architecture. For example, two-dimensional wires and three-dimensional ordered superlattices of $CsPbBr_3$ were synthesized by tuning the precursor concentrations in solutions containing seed nanocrystals (NCs).[5,6] Interparticle electronic coupling in the resulting architectures red-shifted the emission wavelength compared to that of the dispersed NCs and, in superlattices, can lead to superfluorescence.[7] Furthermore, the optical properties of halide perovskite nanowires can be systematically tuned in the visible range by varying the halide composition through postsynthetic halide exchange.[8] Despite successful examples of the self-assembly of metal halide perovskite NCs into superlattices,[9] we still lack a fundamental understanding of the assembly dynamics and outcomes needed to tailor their ensemble properties. Ligand-assisted synthesis of lead halide perovskites often produces nanocubes, which subsequently assemble into regular superlattices and may fuse to form larger single-crystal nanostructures.[10,11] Oriented attachment, which is a growth process in which nanocrystals attach to one another on like faces with crystallographic co-alignment, has been proposed to be the underlying mechanism of anisotropic NC growth.[12,13] For example, oriented attachment was proposed to drive formation of hollow $PbTiO_3$ fibers[14] and $BaTiO_3$ nanocrystals.[15] However, in all of the studies cited above, conclusions concerning the role of oriented attachment were based on postsynthesis observations of the morphology of the nanostructures, but inferring growth pathways from postsynthesis morphological observations can often lead to incorrect conclusions, as shown in a number of crystal systems for which particle assembly was originally proposed as the mechanism of growth.[12,16,17] In these particular cases, highly regular hierarchical morphologies are produced by classical growth processes of atom-by-atom addition complicated by impurity effects acting on atomic steps,[17] growth front instabilities associated with dendrite formation,[16] or nucleation of oriented branches on the surfaces of seed crystals directed by short-range interactions at the seed−electrolyte interface.[18] In contrast, the oriented attachment pathway implies a long-range facet-specific attraction between particles that drives their initial approach and a shorter-range orientation-directing torque that leads to fine adjustment of their mutual orientation before contact.[19] These complex dynamics cannot be unambiguously inferred from an analysis of the final structures alone.

Received: August 24, 2023
Revised: February 23, 2024
Accepted: February 26, 2024
Published: March 5, 2024

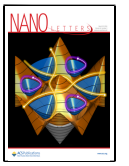

https://doi.org/10.1021/acs.nanolett.3c03189
Nano Lett. 2024, 24, 3299−3306

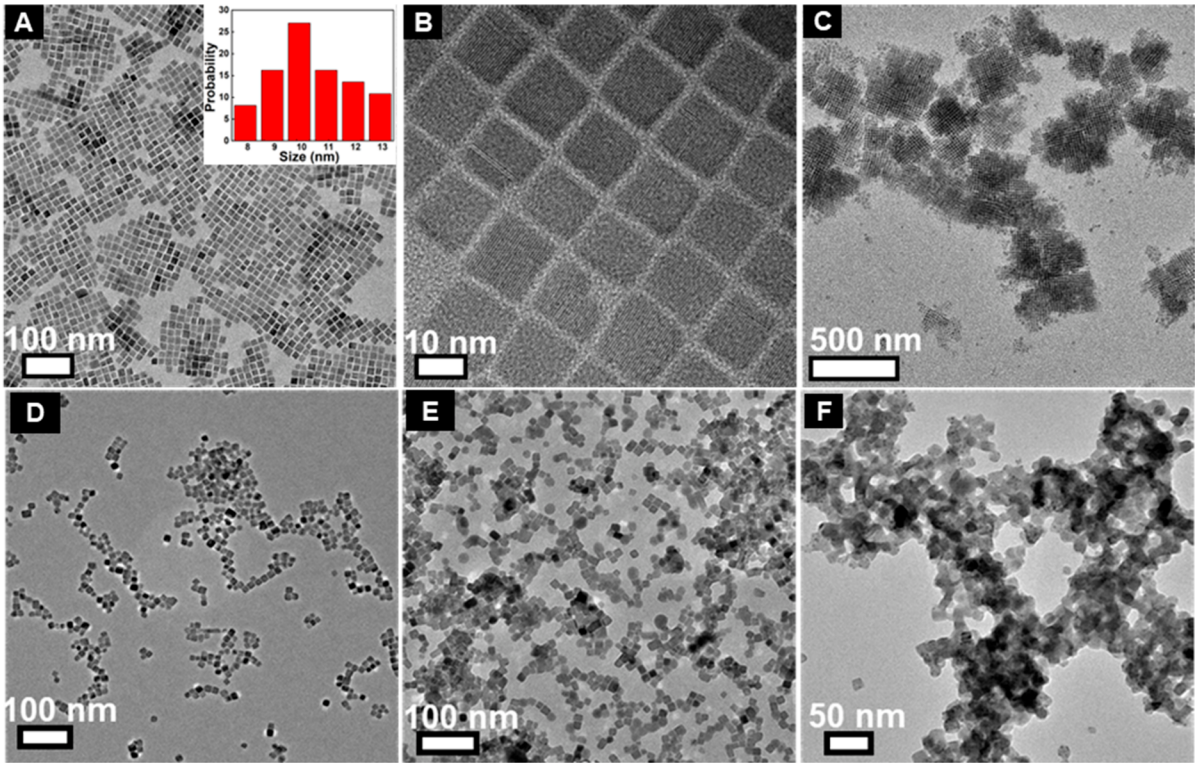

Figure 1. Effect of low-polarity solvents on the aggregation of $CsPbBr_3$ nanocubes. (A and B) TEM and HRTEM images of freshly prepared $CsPbBr_3$ nanocubes in hexane. (C) TEM image of cube-shaped $CsPbBr_3$ NCs in hexane stored under ambient conditions for 2 months. (D) TEM image of freshly prepared cube-shaped $CsPbBr_3$ NCs purified using a low ratio of ethyl acetate to NCs in a colloidal dispersion in toluene (V_{EA}:$V_{toluene}$ = 1:2). (E and F) TEM images of $CsPbBr_3$ NCs using relatively high ratios of ethyl acetate (V_{EA}:$V_{toluene}$ = 1:1 and 2:1, respectively).

Assuming that oriented attachment is indeed responsible for the growth of perovskite nanostructures, another unresolved issue in the case of $CsPbX_3$ is the role of trace polar solvents in promoting anisotropic assembly of $CsPbBr_3$ nanocubes during the ligand-assisted synthesis of nanowires and nanoplates. Two mechanisms have been proposed for the effect of the solvent on cubic $CsPbX_3$ stabilized by a mixture of oleic acid (OA) and oleylamine (OAm). One model proposes that the adsorption of polar solvents on NC surfaces promotes the distortion of the $CsPbI_3$ lattice and thus the transition from a cubic to an orthorhombic structure.[20] This transition, in turn, creates an uncompensated dipole in the nanoparticles, facilitating attachment through dipolar interactions.[20] By comparison of the effect of various solvents, a direct link between the dielectric constant of the solvent and the kinetics of assembly of particles into nanowires has been established. The model, however, does not consider ligand dynamics at the interfaces. Another proposed mechanism encompasses solvent-induced ionization, the desorption of stabilizing ligands from the surface of $CsPbBr_3$ nanocubes, and ligand stabilization of $PbBr_3$- or Br-terminated surfaces of the cubic phase of perovskite.[21] A detailed study of interactions of ligands with perovskite nanocubes revealed that OAm ligands are highly stable and form strong bonds with the $PbBr_3$-rich surface.[22] In contrast, OA ligands can ionize and desorb, thereby exposing the surface to the solvent. These two proposed models are not necessarily mutually exclusive and can be complementary. They address different aspects of particle stabilization and can serve as a basis for a more comprehensive understanding of the interfacial dynamics and forces at the surfaces of the perovskite NCs.

A compelling strategy for obtaining direct evidence of the intermediate states and growth dynamics, including the effects of additives and ligands, involves employing in situ techniques such as in situ transmission electron microscopy (TEM) for real-time observation. In situ TEM has been instrumental in following the attachment dynamics of metal, metal oxide, and metal hydroxide nanoparticles, among others.[23,24] Liquid cell TEM (LCTEM) is unique in its ability to track the motion and trajectories of single NCs in solution at high spatial and temporal resolution, making it a powerful tool for studying the dynamics of nanocrystal growth and assembly in real time. However, using in situ TEM to observe the formation of perovskite nanostructures is challenging. Perovskite NCs are extremely unstable under electron beam irradiation due to the many electron−hole pairs produced by high-energy electrons.[20] Additionally, various side effects such as local heating, momentum transfer from the electron beam, and charging effects come into play. To overcome this challenge, very low dose rates and short exposure times must be used.

In this paper, $CsPbBr_3$ NC motion and orientation are tracked and studied in quantitative detail using LCTEM in combination with ex situ high-resolution TEM (HRTEM). We also compare the effect of various polar solvents on the anisotropic growth of $CsPbBr_3$ NCs by oriented attachment and explore the mechanism by which trace polar solvents direct the growth. The results provide strong evidence that $CsPbBr_3$ NC ripening in solution occurs mainly via oriented attachment and that the adsorption of polar molecules onto the surfaces of $CsPbBr_3$ nanocubes imposes additional directionality on the interparticle interactions, promoting the

https://doi.org/10.1021/acs.nanolett.3c03189
Nano Lett. 2024, 24, 3299−3306

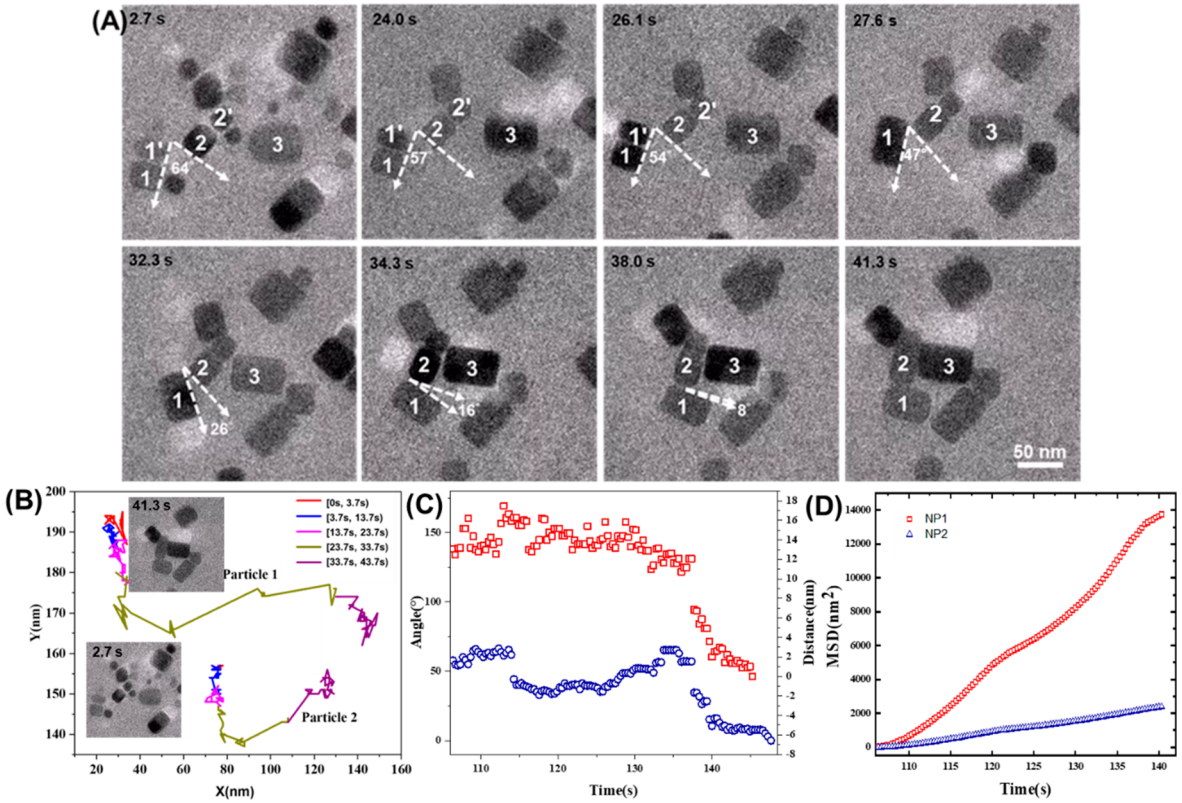

Figure 2. Dynamics of $CsPbBr_3$ NCs before and after coalescence. (A) Time sequence TEM images showing particle diffusion and attachment from Movie S1. (B) Trajectories of NC1 and NC2 in the liquid film recorded for 44 s. Data points denote the location of the particle center. (C) Temporal evolution of the relative angles and distances between the particles. (D) Time dependence of the mean-square displacement (MSD) of particles NC1 and NC2.

growth of single-crystal nanowires or nanowires with antiphase boundaries.

$CsPbBr_3$ NCs capped with OA and OAm ligands were prepared and dispersed in hexane using previously reported methods.[6] HRTEM indicates that the as-synthesized $CsPbBr_3$ NCs have a cubic morphology and a narrow size distribution (d_{ave}) of 10.7 ± 1.5 nm (Figure 1A,B). The nanocubes were stable in hexane for extended periods of time, but some particle aggregation was observed over 2 months due to partial evaporation of the solvent (Figure 1C).

To investigate the dynamic behavior of NCs in a suitable solvent by LCTEM, we first characterize the aggregation state of nanocrystals in mixed solvents of toluene and ethyl acetate over a range of ratios. The addition of ethyl acetate (EA) at a V_{EA}:$V_{toluene}$ volume ratio of 1:2 resulted in the breakdown of the superlattice structure while preserving the cubic shape of the nanocrystals (Figure 1D). An increase in EA content (V_{EA}:$V_{toluene}$ = 1:1 and 2:1) led to NC agglomeration, presumably by further desorption of the ligand from the surface of the $CsPbBr_3$ NCs (Figure 1E,F). Consequently, we chose ethyl acetate and toluene (1:2) as the solvents for LCTEM studies.

The particle attachment process was first studied in a mixture of toluene and ethyl acetate at an extremely low electron dose rate of 0.03 e $Å^{-2}$ s^{-1}, where no electron beam damage of the NCs or changes in their crystallographic structure were detected (Figure S1). To follow the particle assembly process, representative NCs are labeled with numbers 1, 1′, 2, 2′, and 3 on the sequential TEM images in Figure 2A. Initially, the $CsPbBr_3$ NCs had low mobility on the plasma-treated negatively charged SiN_x membrane. After electron beam irradiation for 20 s, particle adhesion weakened, likely due to irradiation-induced negative charging of the NCs,[25,26] and the particles became more mobile within a quasi-two-dimensional layer close to the SiN_x membrane. It is important to emphasize that the charging of nanoparticles irradiated by an electron beam does not alter their crystallographic structure as evidenced by the consistent diffraction pattern observed before and after a 20 min irradiation (Figure S3). At the start of imaging, NC1 and NC2 were already aligned with NC1′ and NC2′, respectively, and both of these pairs fused together within ∼30 s. Over a period of 20 s from the start of imaging, NC1 rotated with respect to NC2 to reduce the relative angle between their edges. Once NC1 and NC2 were aligned, they fused together to form a single crystal, thus completing a third oriented attachment event. The formation of a single crystal is substantiated by ex situ TEM images, which show continuous crystallographic lattices (Figure S2).

By analyzing the changes in the x and y coordinates over time (Figure 2B and Movie S1), we observed that initially NP1 and NP2 undergo correlated translation along the y direction while retaining an almost constant center-to-center distance. At ∼30 s, both NPs change the direction of their motion. NP1 translates along the x direction, while NP2 rotates and translates toward NP1 into a corner-to-corner contact. In the final stage preceding particle attachment, ∼38 s, NP1 rotates into contact with NP2 while both particles translate in the y direction. It is noteworthy that some variation in particle contrast is observed during in situ imaging, indicating NP mobility in the z direction. For example, NP1 moves up at 26.1

https://doi.org/10.1021/acs.nanolett.3c03189
Nano Lett. 2024, 24, 3299−3306

s and NP2 at 34.3 s. However, the contrast of both NPs is the same at the final stages of attachment, indicating alignment in all three directions. Movie S2 also shows similar dynamics of particle aggregation.

To quantify the dynamics of particle approach and shape evolution, we calculated the relative angle and edge−edge distance between NC1 and NC2 before fusion. As shown in Figure 2C, the distance and relative angle fluctuate at early times. Subsequently, NC1 and NC2 exhibit a prolonged period of correlated approach and alignment, followed by coalescence. These dynamics are characteristic of oriented attachment observed in other materials.[12]

To explore the influence of the neighboring particles on the motions of NC1 and NC2, we plotted the time evolution of the mean-square displacement (MSD) for NC1 and NC2 (Figure 2D). The MSD of both particles increases approximately linearly with time. However, the diffusive mobility of NC1, which has only one neighbor, is higher than that of NC2, which is adjacent to a chain of three other NCs. These observations indicate that interactions with neighboring particles reduce the mobility of NC2, likely by enhancing the cumulative adhesion to the substrate as compared to that of the relatively isolated NC1.

Some attachment events involving blocks of assembled particles exhibited a stepwise approach to attachment marked by rapid jumps separated by quiescent periods (Figure 3A,B).

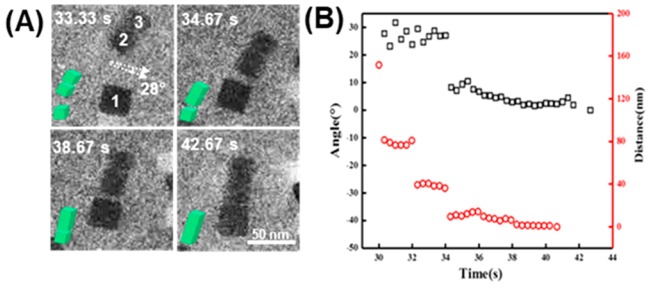

Figure 3. Dynamics of $CsPbBr_3$ nanocrystals before and after coalescence. (A) Time sequence TEM images showing particle diffusion and attachment to a nanorod. (B) Time dependence of relative angles and distances between particles.

For example, NC2 and NC3 jumped as a group toward NC1, forming an angle of 7° between the surfaces of NC2 and NC1 at a 4 nm separation. This dynamics is typical of the oriented attachment process observed in other systems, in which after initial diffusion into the metastable minimum in the solvent separated state particles undergo fine alignment before jump to contact and fusion.[12,27,28] Tracking the changes in the distance and relative angle between NC1 and NC2 before coalescence (Figure 3B) revealed the stepwise dynamics of the approach of the NC2−NC3 particle pair to NC1. The edge−edge distance exhibited three steps separated by abrupt jumps, followed by a gradual approach before contact. After the initial contact at 7°, the NC2−NC3 particle pair and NC1 rotated slightly to achieve co-alignment (Figure 3A).

On the basis of combined in situ and ex situ TEM observations, we hypothesize that the formation of $CsPbBr_3$ nanorods is driven by the desorption of OA−OAm pairs from the nanocube surfaces under electron beam irradiation,[23,29,30] schematically illustrated in Scheme 1. Moreover, our LCTEM studies showed that the tendency for particle aggregation can be tuned by the addition of a polar solvent (ethyl acetate). To understand the effect of changing the solvent, the interactions of the ligands with the NC surfaces and the solvent must be considered.

Scheme 1. Growth of $CsPbBr_3$ Nanorods under Electron Beam Irradiation

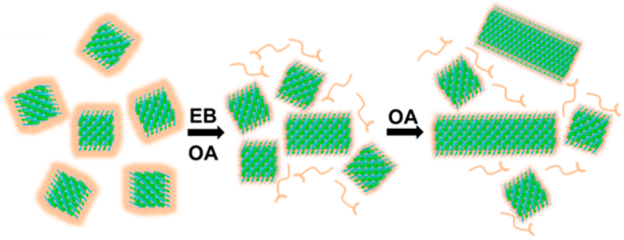

Previous nuclear magnetic resonance studies showed that proton exchange between OAm and OA ligands at the surfaces of $CsPbBr_3$ NCs creates $OAmH^+$ and OA^- species.[21] Protonated $OAmH^+$ then coordinates with Br^- anions and OA^- with Pb^{2+} cations of the perovskite. In the presence of a polar solvent, OA^- ions may solvate and detach from the surface of the NC. Another proposed mechanism is further proton exchange that produces inert neutral species leading to ligand detachment.[31,32] These studies revealed that non-protonated OAm forms strong bonds with surface Pb^{2+} ions and stabilizes $PbBr_3$-rich surfaces.[21] We hypothesize that the addition of a solvent with moderate to high polarity can shift the ligand-binding equilibrium toward ligand solvation, causing partial desorption of the ligands from the NCs. It has been demonstrated in previous work that adjusting the solvent polarity can fine-tune ligand bonding to the perovskite nanocrystal surface, thereby exerting control over the surface ligand density on perovskite nanocrystals.[33−35]

To test the hypothesis presented above, we investigated the effect of polar solvents on the crystallization of $CsPbBr_3$ by monitoring the growth process for 3 h in mixtures of toluene and different polar solvents, such as methanol (1%), ethanol (1%), isopropyl alcohol (IPA, 1%), and water (0.2%, 0.5%, and 1%) (Figure 4A−F and Figures S4−S9). The results show that most NCs self-assemble into nanorods and nanowires with lengths that depend on the polarity of the solvents. The relative polarities of the solvents, determined from shifts in the absorption spectra of organic chromophores,[36] are listed in Table 1, which also shows the average length of the final nanorods in each solvent. It is obvious that the nanorod length increases with the polarity of the solvents, indicating that the strength of the interactions between the ligand and $CsPbBr_3$ NPs is indeed sensitive to solvent polarity.

HRTEM showed that the nanowires were single crystals consisting of smaller co-aligned domains and had a lattice d spacing of ∼0.41 nm (Figure 4G,H and Figure S2D), which is consistent with the d spacing between the (110) planes of cubic $CsPbBr_3$. This consistency in d spacing affirms that the nanorod retains the crystal structure of cubic $CsPbBr_3$. Local chemical changes at the nanoparticle surface drive facet specificity and hence the directionality of interparticle forces, which has been reported previously by our group.[37,38] Recent computational studies predicted that water molecules adsorb to PbBr- and CsBr-terminated surfaces of cubic $CsPbBr_3$ with similar adsorption energies of −0.51 and −0.62 eV, respectively.[39] However, charge transfer from the perovskite surfaces to the adsorbed water molecules has the opposite sign. According to a Bader analysis, the charge transfer is −0.020 e

https://doi.org/10.1021/acs.nanolett.3c03189
Nano Lett. 2024, 24, 3299−3306

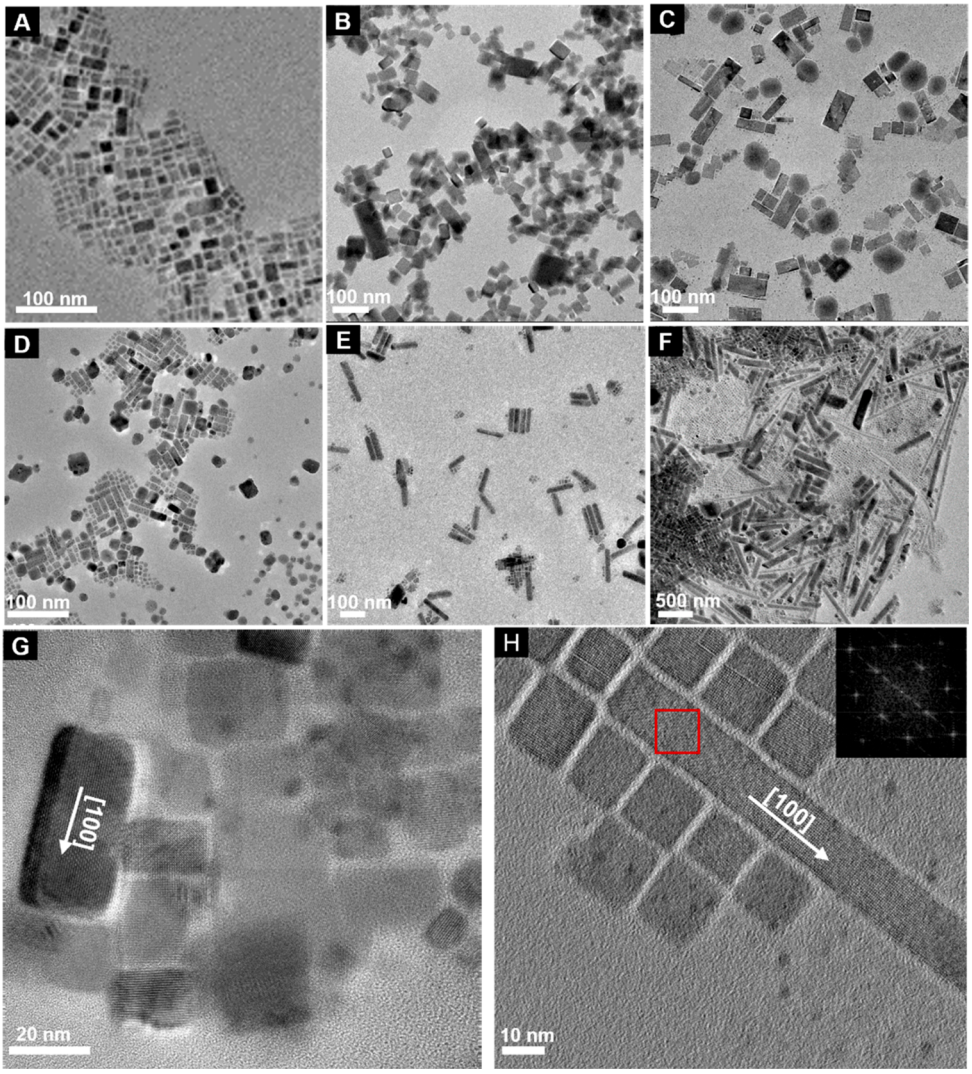

Figure 4. TEM images showing oriented attachment of $CsPbBr_3$ NCs regulated by solvent: (A) IPA (1%), (B) ethanol (1%), (C) methanol (1%), (D) H_2O (0.2%), (E) H_2O (0.5%), and (F) H_2O (1.0%). (G) HRTEM image of a nanorod obtained in 0.2% H_2O. (H) HRTEM image of a nanowire obtained in 0.5% H_2O. The inset shows fast Fourier transform (FFT) analysis of the area highlighted with the red square containing the region of fusion of two nanorods.

Table 1. Relative Polarities of the Solvents and Average Lengths of the Final Nanorod in Different Solvents

	toluene	ethyl acetate	2-propanol	ethanol	methanol	water	water	water
	–	33:67[a]	1:99[a]	1:99[a]	1:99[a]	0.2:99.8[a]	0.5:99.5[a]	1:99[a]
polarity[b]	0.099	0.228	0.546	0.654	0.762	1	1	1
particle length (nm)[c]	9 ± 1	13 ± 4	24 ± 5	66 ± 20	82 ± 43	25 ± 4	143 ± 28	248 ± 126

[a]Solvent:toluene ratio. [b]Polarities taken from ref 19. [c]The average length of particles was calculated on the basis of 100 measurements.

from the PbBr-terminated surface and +0.039 e from the CsBr-terminated surface. Thereby, the local dipole moments at the PbBr–water and CsBr–water interfaces point in opposite directions, creating the potential for dipole–dipole interactions to provide both an attractive force and an aligning torque that can drive self-assembly of $CsPbBr_3$ nanocubes into single-crystalline nanowires through oriented attachment, as shown in Scheme 2. Ligand desorption, which can be induced by a nelectron beam or competition with polar solvents, was predicted to increase the density of the surface dipole on $CsPbBr_3$ nanoparticles.[40] The average range of interparticle dipolar interactions defined as the maximum separation, at which the dipolar energy is larger than the thermal energy at room temperature (kT), is 40 nm for fully functionalized NPs and 47 nm for pristine 10 nm NPs. The corresponding

Scheme 2. Polar Solvents Drive Self-Assembly of $CsPbBr_3$ Nanocubes into Single-Crystalline Nanowires through Oriented Attachment

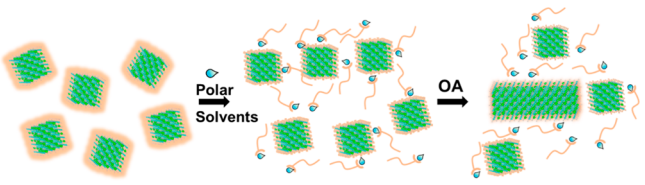

https://doi.org/10.1021/acs.nanolett.3c03189
Nano Lett. 2024, 24, 3299–3306

strength of attractive interactions between 10 nm nanoparticles is calculated to increase from −8.4 kT for fully functionalized to −13.4 kT for pristine nanoparticle surfaces at a 20 nm separation (Figure S10).

Growth by oriented attachment due to dipole−dipole interactions was previously reported for ZnO, for which a permanent dipole along the (001) direction drives primary NCs to assemble into (001)-oriented nanowires.[12] In the results presented above for $CsPbBr_3$, the strength of the dipolar interactions should be controlled by both the dielectric properties of the various polar solvents and the degree to which those solvents lead to ligand desorption and consequent polarization of the NCs, thus providing a rationale for the observed solvent effect. With the increasing polarity going from IPA to ethanol, methanol, and water, the extent of solvent-induced polarization of $CsPbBr_3$ increases, resulting in the formation of single-crystalline elongated nanorods through the oriented attachment of NCs, as evidenced by fast Fourier transform (FFT) analysis (Figure 4H, inset), though the formation of antiphase defects cannot be ruled out.

A clear correlation between the polarity of the co-solvent and the length of $CsPbBr_3$ nanorods illuminates the profound impact of polar solvents on the directional interactions between $CsPbBr_3$ nanocubes. In the absence of polar solvents, the ligands tightly adhere to the nanocube surfaces, forming an obstructive barrier that hinders their proximity and attachment (Figure 1A,B).[23,41] However, the introduction of a polar solvent into the system marks a critical juncture. In polar solvents, the interplay between the ligands and solvent molecules becomes energetically advantageous, weakening the bonds between the ligands and nanocubes. For example, the energies for the adsorption of water onto PbBr- and CsBr-terminated surfaces are similar or higher than the corresponding adsorption energies of octanoic acid ligands of −0.56 and −0.48 eV, respectively, representative of oleic acid and OAm.[42] Consequently, the ligands gradually disengage from the nanocube surfaces, permitting NCs to assemble in a specific orientation. This oriented attachment, guided by the controlled detachment of ligands, results in the formation of nanorods that exhibit a pronounced alignment along specific crystallographic axes, notably the (100) direction. The degree of preference for attachment along the (100) direction increases with solvent polarity, which is evident from the elongation of nanowires in response to the increased solvent polarity (Figure 4A−C) or water concentration (Figure 4D−F).

In summary, in situ studies of the dynamics of $CsPbBr_3$ NCs in solution have revealed directional motion with a gradual approach and alignment separated by translational and rotational jumps characteristic of oriented attachment. These findings identify ionization-induced desorption of ligands as the likely primary driver for the oriented attachment of perovskite nanocubes. By the addition of solvents with moderate to high polarity to the CsPbBr$_3$ NC solution, we could systematically tune the interaction between the ligands and the NCs to control the rate of oriented attachment. The opposite direction of the charge transfer at the PbBr−water and CsBr−water interfaces directs the oriented assembly of these two perovskite surfaces and promotes the growth of single-crystal nanowires via dipolar-driven oriented attachment. These findings provide new insights into the activity and interaction of perovskite nanocrystals in solution, which is greatly important for knowledge-based control of the morphology and properties of perovskite materials. They further contribute to advances in the application of perovskites in high-performance optoelectronic devices.

■ ASSOCIATED CONTENT

Supporting Information

The Supporting Information is available free of charge at https://pubs.acs.org/doi/10.1021/acs.nanolett.3c03189.

Materials and methods, characterization (photoluminescence spectra and TEM experiments), data analysis and interparticle dipolar interactions, Table S1, Figures S1−S10, and captions for movies (PDF)

$CsPbBr_3$ NCs diffuse and attach to irregular shapes in liquid at a dose rate of 0.03 e Å^{-2} s^{-1} (Movie S1) (AVI)

Dynamic behavior of $CsPbBr_3$ NCs during aggregation (Movie S2) (AVI)

■ AUTHOR INFORMATION

Corresponding Authors

Maria L. Sushko − *Physical Sciences Division, Pacific Northwest National Laboratory, Richland, Washington 99352, United States;* orcid.org/0000-0002-7229-7072; Email: Maria.sushko@pnnl.gov

Lili Liu − *Physical Sciences Division, Pacific Northwest National Laboratory, Richland, Washington 99352, United States;* orcid.org/0000-0002-9595-4303; Email: Lili.liu@pnnl.gov

Authors

Kyle Kluherz − *Department of Chemistry, University of Washington, Seattle, Washington 98195, United States*

Biao Jin − *Physical Sciences Division, Pacific Northwest National Laboratory, Richland, Washington 99352, United States;* orcid.org/0000-0002-4008-6414

Daniel R. Gamelin − *Department of Chemistry, University of Washington, Seattle, Washington 98195, United States;* orcid.org/0000-0003-2888-9916

James J. De Yoreo − *Physical Sciences Division, Pacific Northwest National Laboratory, Richland, Washington 99352, United States; Department of Materials Science and Engineering, University of Washington, Seattle, Washington 98185, United States;* orcid.org/0000-0002-9541-733X

Complete contact information is available at: https://pubs.acs.org/10.1021/acs.nanolett.3c03189

Notes

The authors declare no competing financial interest.

■ ACKNOWLEDGMENTS

This material is based upon work supported by the Department of Energy (DOE), Office of Science, Basic Energy Sciences, Division of Materials Sciences and Engineering (FWP12152), at Pacific Northwest National Laboratory (PNNL). All LPTEM work was performed in the Environmental Molecular Sciences Laboratory (EMSL), which is an Office of Biological and Environmental Research user facility located at PNNL. PNNL is operated by Battelle for the Department of Energy under Contract DEAC05-76RLO1830. D.R.G. acknowledges support from the University of Washington Molecular Engineering Materials Center, a National Science Foundation Materials Research Science and Engineering Center (Grants DMR-2308979 and DMR-

1719797). K.K. gratefully acknowledges support from the U.S. Department of Energy Office of Science Graduate Student Research (SCGSR) program, administered by the Oak Ridge Institute for Science and Education (ORISE) for the DOE.

REFERENCES

(1) Protesescu, L.; Yakunin, S.; Bodnarchuk, M. I.; Krieg, F.; Caputo, R.; Hendon, C. H.; Yang, R. X.; Walsh, A.; Kovalenko, M. V. Nanocrystals of cesium lead halide perovskites ($CsPbX_3$, X = Cl, Br, and I): novel optoelectronic materials showing bright emission with wide color gamut. *Nano Lett.* **2015**, *15*, 3692−3696.

(2) Huang, H.; Feil, M. W.; Fuchs, S.; Debnath, T.; Richter, A. F.; Tong, Y.; Wu, L.; Wang, Y.; Döblinger, M.; Nickel, B. Growth of perovskite $CsPbBr_3$ nanocrystals and their formed superstructures revealed by in situ spectroscopy. *Chem. Mater.* **2020**, *32*, 8877−8884.

(3) Yao, E. P.; Bohn, B. J.; Tong, Y.; Huang, H.; Polavarapu, L.; Feldmann, J. Exciton diffusion lengths and dissociation rates in $CsPbBr_3$ nanocrystal−fullerene composites: layer-by-layer versus blend structures. *Adv. Opt. Mater.* **2019**, *7*, 1801776.

(4) Dey, A.; Ye, J.; De, A.; Debroye, E.; Ha, S. K.; Bladt, E.; Kshirsagar, A. S.; Wang, Z.; Yin, J.; Wang, Y.; et al. State of the art and prospects for halide perovskite nanocrystals. *ACS Nano* **2021**, *15*, 10775−10981.

(5) Tong, Y.; Yao, E. P.; Manzi, A.; Bladt, E.; Wang, K.; Doeblinger, M.; Bals, S.; Müller-Buschbaum, P.; Urban, A.; Lakshminarayana, P.; et al. Spontaneous self-assembly of perovskite nanocrystals into electronically coupled supercrystals: toward filling the green gap. *Adv. Mater.* **2018**, *30*, 1801117.

(6) Tong, Y.; Bohn, B. J.; Bladt, E.; Wang, K.; Müller-Buschbaum, P.; Bals, S.; Urban, A. S.; Polavarapu, L.; Feldmann, J. From precursor powders to $CsPbX_3$ perovskite nanowires: One-pot synthesis, growth mechanism, and oriented self-assembly. *Angew. Chem., Int. Ed.* **2017**, *56*, 13887−13892.

(7) Rainò, G.; Becker, M. A.; Bodnarchuk, M. I.; Mahrt, R. F.; Kovalenko, M. V.; Stöferle, T. Superfluorescence from lead halide perovskite quantum dot superlattices. *Nature* **2018**, *563*, 671−675.

(8) Tang, Y.; Poonia, D.; van der Laan, M.; Timmerman, D.; Kinge, S.; Siebbeles, L. D. A.; Schall, P. Electronic coupling of highly ordered perovskite nanocrystals in supercrystals. *ACS Appl.Energy Mater.* **2022**, *5*, 5415−5422.

(9) Cherniukh, I.; Rainò, G.; Stöferle, T.; Burian, M.; Travesset, A.; Naumenko, D.; Amenitsch, H.; Erni, R.; Mahrt, R. F.; Bodnarchuk, M. I.; et al. Perovskite-type superlattices from lead halide perovskite nanocubes. *Nature* **2021**, *593*, 535−542.

(10) Patra, B. K.; Agrawal, H.; Zheng, J.-Y.; Zha, X.; Travesset, A.; Garnett, E. C. Close-packed ultrasmooth self-assembled monolayer of $CsPbBr_3$ perovskite nanocubes. *ACS Appl. Mater. Interfaces* **2020**, *12*, 31764−31769.

(11) Liu, Y.; Zheng, X.; Fang, Y.; Zhou, Y.; Ni, Z.; Xiao, X.; Chen, S.; Huang, J. Ligand assisted growth of perovskite single crystals with low defect density. *Nat. Commun.* **2021**, *12*, 1686.

(12) Liu, L.; Nakouzi, E.; Sushko, M. L.; Schenter, G. K.; Mundy, C. J.; Chun, J.; De Yoreo, J. J. Connecting energetics to dynamics in particle growth by oriented attachment using real-time observations. *Nat. Commun.* **2020**, *11*, 1045.

(13) Li, D.; Nielsen, M. H.; Lee, J. R. I.; Frandsen, C.; Banfield, J. F.; De Yoreo, J. J. Direction-specific interactions control crystal growth by oriented attachment. *Science* **2012**, *336*, 1014−1018.

(14) Rørvik, P.; Almli, A.; van Helvoort, A. T. J.; Holmestad, R.; Tybell, T.; Grande, T.; Einarsrud, M. A. $PbTiO_3$ nanorod arrays grown by self-assembly of nanocrystals. *Nanotechnology* **2008**, *19*, 225605.

(15) Yasui, K.; Kato, K. Oriented Attachment of Cubic or Spherical $BaTiO_3$ Nanocrystals by van der Waals Torque. *J. Phys. Chem. C* **2015**, *119*, 24597−24605.

(16) Liu, L.; Zhang, S.; Bowden, M. E.; Chaudhuri, J.; Yoreo, J. J. D. In Situ TEM and AFM investigation of morphological controls during the growth of single crystal $BaWO_4$. *Cryst. Growth Des.* **2018**, *18*, 1367−1375.

(17) Smeets, P. J. M.; Cho, K. R.; Sommerdijk, N. A. J. M.; De Yoreo, J. J. A mesocrystal-like morphology formed by classical polymer-mediated crystal growth. *Adv. Funct. Mater.* **2017**, *27*, 1701658.

(18) Liu, L.; Sushko, M. L.; Buck, E. C.; Zhang, X.; Kovarik, L.; Shen, Z.; Tao, J.; Nakouzi, E.; Liu, J.; De Yoreo, J. J. Revisiting the growth mechanism of hierarchical semiconductor nanostructures: The role of secondary nucleation in branch formation. *J. Phys. Chem. L* **2019**, *10*, 6827−6834.

(19) Sushko, M. L. Crystallization pathways and interfacial drivers for the formation of hierarchical architectures. *J. Cryst. Growth* **2022**, *600*, 126914.

(20) Sun, J. K.; Huang, S.; Liu, X. Z.; Xu, Q.; Zhang, Q. H.; Jiang, W. J.; Xue, D. J.; Xu, J. C.; Ma, J. Y.; Ding, J.; et al. Polar solvent induced lattice distortion of cubic $CsPbI_3$ nanocubes and hierarchical self-assembly into orthorhombic single-crystalline nanowires. *J. Am. Chem. Soc.* **2018**, *140*, 11705−11715.

(21) Zhong, Q.; Cao, M.; Xu, Y.; Li, P.; Zhang, Y.; Hu, H.; Yang, D.; Xu, Y.; Wang, L.; Li, Y.; et al. L-type ligand-assisted acid-free synthesis of $CsPbBr_3$ Nanocrystals with near-unity photoluminescence quantum yield and high stability. *Nano Lett.* **2019**, *19*, 4151−4157.

(22) Fiuza-Maneiro, N.; Sun, K.; López-Fernández, I.; Gómez-Graña, S.; Müller-Buschbaum, P.; Polavarapu, L. Ligand Chemistry of Inorganic Lead Halide Perovskite Nanocrystals. *ACS Energy Lett.* **2023**, *8*, 1152−1191.

(23) Liu, L.; Song, D.; Jin, B.; Sinnwell, M. A.; Liu, J.; De Yoreo, J. J.; Sushko, M. L. Role of the solvent−surfactant duality of ionic liquids in directing two-dimensional particle assembly. *J. Phys. Chem. C* **2020**, *124*, 24215−24222.

(24) Liu, L.; Kruska, K.; Hall, G. B.; Clark, R. A.; Meier, D. E.; Buck, E. C. Formation and growth of cerium (III) oxalate nanocrystals by liquid-cell transmission electron microscopy. *Scr. Mater.* **2022**, *219*, 114856.

(25) Zheng, H.; Claridge, S. A.; Minor, A. M.; Alivisatos, A. P.; Dahmen, U. Nanocrystal diffusion in a liquid thin film observed by in situ transmission electron microscopy. *Nano Lett.* **2009**, *9*, 2460−2465.

(26) Bakalis, E.; Parent, L. R.; Vratsanos, M.; Park, C.; Gianneschi, N. C.; Zerbetto, F. Complex nanoparticle diffusional motion in liquid-cell transmission electron microscopy. *J. Phys. Chem. C* **2020**, *124*, 14881−14890.

(27) Sushko, M. L. Understanding the driving forces for crystal growth by oriented attachment through theory and simulations. *J. Mater. Res.* **2019**, *34*, 2914−2927.

(28) Sushko, M. L.; Rosso, K. M. The origin of facet selectivity and alignment in anatase TiO_2 nanoparticles in electrolyte solutions: implications for oriented attachment in metal oxides. *Nanoscale* **2016**, *8*, 19714−19725.

(29) Song, M.; Zhou, G.; Lu, N.; Lee, J.; Nakouzi, E.; Wang, H.; Li, D. Oriented attachment induces fivefold twins by forming and decomposing high-energy grain boundaries. *Science* **2020**, *367*, 40−45.

(30) Dissanayake, T. U.; Wang, M.; Woehl, T. J. Revealing reactions between the electron beam and nanoparticle capping ligands with correlative fluorescence and liquid-phase electron microscopy. *ACS Appl. Mater. Interfaces* **2021**, *13*, 37553−37562.

(31) De Roo, J.; Ibáñez, M.; Geiregat, P.; Nedelcu, G.; Walravens, W.; Maes, J.; Martins, J. C.; Van Driessche, I.; Kovalenko, M. V.; Hens, Z. Highly dynamic ligand binding and light absorption coefficient of cesium lead bromide perovskite panocrystals. *ACS Nano* **2016**, *10*, 2071−2081.

(32) Almeida, G.; Goldoni, L.; Akkerman, Q.; Dang, Z.; Khan, A. H.; Marras, S.; Moreels, I.; Manna, L. Role of acid−base equilibria in the size, shape, and phase control of cesium lead bromide nanocrystals. *ACS Nano* **2018**, *12*, 1704−1711.

(33) Jia, D.; Chen, J.; Qiu, J.; Ma, H.; Yu, M.; Liu, J.; Zhang, X. Tailoring solvent-mediated ligand exchange for CsPbI3 perovskite

https://doi.org/10.1021/acs.nanolett.3c03189
Nano Lett. 2024, 24, 3299−3306

quantum dot solar cells with efficiency exceeding 16.5%. *Joule* **2022**, *6*, 1632−1653.
(34) Xue, J.; Lee, J. W.; Dai, Z.; Wang, R.; Nuryyeva, S.; Liao, M. E.; Chang, S. Y.; Meng, L.; Meng, D.; Sun, P.; et al. Surface ligand management for stable $FAPbI_3$ perovskite quantum dot solar cells. *Joule* **2018**, *2*, 1866−1878.
(35) Jin, X.; Ma, K.; Gao, H. Tunable luminescence and enhanced polar solvent resistance of perovskite nanocrystals achieved by surface-initiated photopolymerization. *J. Am. Chem. Soc.* **2022**, *144*, 20411−20420.
(36) Reichardt, C.; Welton, T. Solvent effects on the absorption spectra of organic compounds. *Solvents and Solvent Effects in Organic Chemistry* **2010**, 359−424.
(37) Cheng, Y.; Tao, J.; Zhu, G.; Soltis, J. A.; Legg, B. A.; Nakouzi, E.; De Yoreo, J. J.; Sushko, M. L.; Liu, J. Near surface nucleation and particle mediated growth of colloidal Au nanocrystals. *Nanoscale* **2018**, *10*, 11907−11912.
(38) Zhu, G.; Sushko, M. L.; Loring, J. S.; Legg, B. A.; Song, M.; Soltis, J. A.; Huang, X.; Rosso, K. M.; De Yoreo, J. J. Self-similar mesocrystals form via interface-driven nucleation and assembly. *Nature* **2021**, *590*, 416−422.
(39) Zhang, X.; Quhe, R.; Lei, M. Insights into the adsorption of water and oxygen on the cubic $CsPbBr_3$ surfaces: A first-principles study. *Chin. Phys. B* **2022**, *31*, No. 046401.
(40) Basera, P.; Traore, B.; Even, J.; Katan, C. Interfacial engineering to modulate surface dipoles, work functions and dielectric confinement of halide perovskites. *Nanoscale* **2023**, *15*, 11884−11897.
(41) Si, K. J.; Chen, Y.; Shi, Q.; Cheng, W. Nanoparticle superlattices: the roles of soft ligands. *Adv. Sci.* **2018**, *5*, 1700179.
(42) Zaccaria, F.; Zhang, B. W.; Goldoni, L.; Imran, M.; Zito, J.; van Beek, B.; Lauciello, S.; De Trizio, L.; Manna, L.; Infante, I. The reactivity of $CsPbBr_3$ nanocrystals toward acid/base ligands. *ACS Nano* **2022**, *16*, 1444−1455.

https://doi.org/10.1021/acs.nanolett.3c03189
Nano Lett. 2024, 24, 3299−3306